
PHASE-SPACE REPRESENTATION OF COHERENT STATES GENERATED THROUGH SUSY QM FOR TILTED ANISOTROPIC DIRAC MATERIALS

Daniel O-Campa^{†,1} and Erik Díaz-Bautista^{†,2}

[†]Escuela Superior de Física y Matemáticas del Instituto Politécnico Nacional, 07738 Mexico City, Mexico.
e-mail: dortizca@ipn.mx¹, ediazba@ipn.mx²

March 29, 2024

ABSTRACT

In this paper, we examine the electron interaction within tilted anisotropic Dirac materials when subjected to external electric and magnetic fields possessing translational symmetry. Specifically, we focus on a distinct non-zero electric field magnitude, enabling the separation of the differential equation system inherent in the eigenvalue problem. Subsequently, employing supersymmetric quantum mechanics facilitates the determination of eigenstates and eigenvalues corresponding to the Hamiltonian operator. To delve into a semi-classical analysis of the system, we identify a set of coherent states. Finally, we assess the characteristics of these states using fidelity and the phase-space representation through the Wigner function.

Keywords: Dirac materials, supersymmetric quantum mechanics, coherent states, fidelity, Wigner function.

1 Introduction

The study of anisotropic Dirac materials with tilted cones has garnered significant attention due to their unique electronic properties and potential applications in various fields of physics [1–7]. These materials are characterized by an effective Hamiltonian that captures the behavior of charge carriers near the Dirac points, incorporating both anisotropy and the tilting of the Dirac cones. This fact has led to an emergent research area in semiconductor technology, valleytronics [8, 9], in which the valley degree of freedom could allow the manipulation of the electronic transport in two-dimensional materials, even in pristine graphene, in which the inversion symmetry of the system prohibits valley-selective excitations [10].

On the other hand, the concept of coherent states, originating from the study of harmonic oscillators, has been extended to Dirac materials in many research works, leading to the formulation of Barut-Girardello coherent states among others [11–13]. It is also well known that in some cases supersymmetric quantum mechanics approach can be used to solve the eigenvalue problem associated with the effective Hamiltonian and allows the construction of lowering operators [14–17], which play a crucial role in the investigation of coherent states and their behavior in phase space. In a different (but not disconnected) vein, the fidelity between an evolved state and its initial state provides insights into the periodic behavior of the system [18]. Likewise, the Wigner function [19], a quasiprobability distribution, offers a unique perspective on the distribution of coherent states in phase space, shedding light on their classical or quantum nature [20–23]. Initially, the Wigner function arose from a quantum mechanics formulation in phase space [24, 25] in which, under certain requirements, it is possible to associate an integrable function defined on \mathbb{R}^{2n} to an operator in a Hilbert space \mathcal{H} through the so-called Weyl transform [26–28]. Nowadays, there are many experimental applications of the Wigner function in quantum transport studies, since it allows a mixed quantum–semi-classical description of the systems [29, 30]. For instance, the Wigner function has been employed in a quantum-tomography approach to reconstruct quantum states of solitary electrons or electric currents [31–37].

With this motivation, this paper presents a systematic exploration of anisotropic Dirac materials with tilted

cones as follows: in section 2 it is introduced the application of supersymmetric quantum mechanics to determine eigenstates and eigenvalues of the Hamiltonian operator assuming a specific electric field amplitude that enables such a task. Then, in section 3 the concept of Barut-Girardello coherent states is discussed. After that, in section 4 the behavior of the Barut-Girardello coherent states is discussed by using fidelity and the Wigner function. Finally, in section 5 we discuss the conclusions.

2 The eigenvalue problem

For those Dirac-like materials that exhibit anisotropy and tilted cones, the charge carriers at low energies are described by the effective Hamiltonian

$$\mathcal{H}_0 = \nu (v_x p_x \sigma_x + v_y p_y \sigma_y + v_t p_y \sigma_0), \quad (1)$$

where $\nu = \pm 1$ is the valley index, v_x and v_y are the anisotropic velocities, and v_t is a velocity term that arises from the tilting of the Dirac cones. Here, $\sigma_{x,y}$ denote the Pauli matrices, σ_0 is the 2×2 identity matrix, and p_x, p_y represent the canonical momentum operator.

If the interaction with stationary but position-dependent magnetic and electric fields is considered, the Hamiltonian in Eq. (1) has to be modified by the minimal coupling rule. Thus, by considering a simplified case where both fields change along one direction (namely x) and the magnetic field $\vec{\mathcal{B}}$ is perpendicular to the surface of the material (the x - y plane), and the electric field $\vec{\mathcal{E}}$ lies in-plane, then the Hamiltonian becomes

$$\mathcal{H} = \nu v_x \left[p_x \sigma_x + \frac{v_y}{v_x} (p_y + \mathcal{A}_y(x)) \sigma_y + \frac{v_t}{v_x} \left(p_y + \mathcal{A}_y(x) - \frac{\nu}{v_t} \phi(x) \right) \sigma_0 \right], \quad (2)$$

where $\vec{\mathcal{A}} = \mathcal{A}_y(x) \hat{e}_y$ is the vector potential such as $\vec{\mathcal{B}} = \nabla \times \vec{\mathcal{A}} = \mathcal{B}(x) \hat{e}_z$ ($\mathcal{B}(x) = \mathcal{A}'_y(x)$), and $\phi(x)$ is the scalar potential such that $\vec{\mathcal{E}} = -\nabla \phi(x) = \mathcal{E}(x) \hat{e}_x$ ($\mathcal{E}(x) = -\phi'(x)$). From this Hamiltonian, it is straightforward that $[\mathcal{H}, p_y] = 0$. Thus, in the eigenvalue equation $\mathcal{H}\Psi(x, y) = E\Psi(x, y)$, the eigenfunctions can be expressed as

$$\Psi(x, y) = e^{iky} \bar{\Psi}(x), \quad (3)$$

where $\bar{\Psi}(x) = (\psi^+(x), i\psi^-(x))^T$. Then, the Hamiltonian acting on $\Psi(x, y)$ becomes

$$\mathcal{H} = \nu v_x \begin{pmatrix} \phi_{\text{eff}}(x) & -i\mathcal{L}^- \\ i\mathcal{L}^+ & \phi_{\text{eff}}(x) \end{pmatrix}, \quad (4)$$

where

$$\begin{aligned} \mathcal{L}^\pm &= \mp \frac{d}{dx} + W(x), \quad W(x) = \frac{v_y}{v_x} (k + \mathcal{A}_y(x)), \\ \phi_{\text{eff}}(x) &= \frac{v_t}{v_x} \left(k + \mathcal{A}_y(x) - \frac{\nu}{v_t} \phi(x) \right). \end{aligned} \quad (5)$$

In this way, the eigenvalue equation leads to the following system

$$\mathcal{L}^\pm \psi^\pm(x) = \nu \left(\frac{E}{v_x} - \nu \phi_{\text{eff}}(x) \right) \psi^\mp(x). \quad (6)$$

Now, by applying once again the \mathcal{L}^\mp operator on both sides of the equation, it turns out to be

$$H^\pm \psi^\pm(x) = \left(\frac{E}{v_x} - \nu \phi_{\text{eff}}(x) \right)^2 \psi^\pm(x) \mp \phi'_{\text{eff}}(x) \psi^\mp(x), \quad (7)$$

where H^\pm are two one-dimensional Schrödinger Hamiltonian operators that factorize as:

$$H^\pm = \mathcal{L}^\mp \mathcal{L}^\pm = -\frac{d^2}{dx^2} + V^\pm(x), \quad \text{with } V^\pm(x) = W^2(x) \pm W'(x). \quad (8)$$

Note that Eq. (7) leads to second-order coupled differential equations for the $\psi^\pm(x)$ components that are not easily decoupled due to the source-like term $\phi'_{\text{eff}}(x)$. Nevertheless, to make the term that couples the differential system in Eq. (7) vanish, we can choose $\phi'_{\text{eff}}(x) = 0$, which can be guaranteed if the amplitudes of the electric and magnetic fields satisfy the relationship:

$$\mathcal{E}(x) = -\nu v_t \mathcal{B}(x). \quad (9)$$

In this scenario, the effective potential becomes constant:

$$\phi_{\text{eff}}(x) = \frac{v_t}{v_x} k. \quad (10)$$

Note that the suitable choice of the scalar potential $\phi(x)$ not only allows us to decouple the system of differential equations but also enables us to express information about the tilting of the cones as an energy level shift. This results in the creation of a band gap between the conduction and valence bands.

Moreover, in this way, the system of differential equations in (7) decouples as follows:

$$H^\pm \psi^\pm(x) = \epsilon \psi^\pm(x), \quad \epsilon = \left(\frac{E - \nu v_t k}{v_x} \right)^2. \quad (11)$$

On the other hand, from eq. (8), the Hamiltonians H^\pm fulfill that

$$H^\pm \mathcal{L}^\mp = \mathcal{L}^\mp H^\mp. \quad (12)$$

This relationship indicates that H^\pm are supersymmetric partner Hamiltonians [14, 15, 18]. Consequently, the eigenvalues ϵ_n^+ and eigenfunctions $\psi_n^+(x)$ of H^+ can be determined if those of H^- , i.e., ϵ_n^- and $\psi_n^-(x)$, are known, and vice versa. This can lead to one of the following three cases:

i) If $\mathcal{L}^- \psi_0^-(x) = 0$, then $\epsilon_0^- = 0$ and

$$\psi_n^+(x) = \frac{\mathcal{L}^- \psi_{n+1}^-(x)}{\sqrt{\epsilon_{n+1}^-}}, \quad \text{for } n = 0, 1, \dots \quad (13)$$

with eigenvalue $\epsilon_n^+ = \epsilon_{n+1}^-$. Therefore, the eigenfunctions and eigenvalues of the Hamiltonian \mathcal{H} are given by

$$\Psi_n(x, y) = \frac{e^{iky}}{\sqrt{2^{1-\delta_{n,0}}}} \begin{pmatrix} (1 - \delta_{n,0}) \psi_{n-1}^+(x) \\ i \psi_n^-(x) \end{pmatrix}, \quad E_n = \nu v_t k + \kappa v_x \sqrt{\epsilon_n^-} \quad \text{for } n = 0, 1, \dots \quad (14)$$

being $\kappa = \pm 1$ the band index for electrons (1) and holes (-1), respectively.

ii) If $\mathcal{L}^+ \psi_0^+(x) = 0$, then $\epsilon_0^+ = 0$ and

$$\psi_n^-(x) = \frac{\mathcal{L}^+ \psi_{n+1}^+(x)}{\sqrt{\epsilon_{n+1}^+}}, \quad \text{for } n = 0, 1, \dots \quad (15)$$

with eigenvalue $\epsilon_n^- = \epsilon_{n+1}^+$. Therefore, the eigenfunctions and eigenvalues of the Hamiltonian \mathcal{H} are given by

$$\Psi_n(x, y) = \frac{e^{iky}}{\sqrt{2^{1-\delta_{n,0}}}} \begin{pmatrix} \psi_n^+(x) \\ i(1 - \delta_{n,0}) \psi_{n-1}^-(x) \end{pmatrix}, \quad E_n = \nu v_t k + \kappa v_x \sqrt{\epsilon_n^+} \quad \text{for } n = 0, 1, \dots \quad (16)$$

iii) If $\mathcal{L}^+ \psi_0^+(x) \neq 0$ and $\mathcal{L}^- \psi_0^-(x) \neq 0$, then the ground state of both Hamiltonians H^\pm has energy different from zero. Moreover, it is fulfilled that

$$\psi_n^\pm(x) = \frac{\mathcal{L}^\mp \psi_n^\mp(x)}{\sqrt{\epsilon_n}}, \quad \text{for } n = 0, 1, \dots \quad (17)$$

with eigenvalue $\epsilon_n^- = \epsilon_n^+ = \epsilon_n$. Therefore, the eigenfunctions and eigenvalues of the Hamiltonian \mathcal{H} are given by

$$\Psi_n(x, y) = \frac{e^{iky}}{\sqrt{2}} \begin{pmatrix} \psi_n^+(x) \\ i \psi_n^-(x) \end{pmatrix}, \quad E_n = \nu v_t k + \kappa v_x \sqrt{\epsilon_n} \quad \text{for } n = 0, 1, \dots \quad (18)$$

We must emphasize that each of these cases depends solely on the choice of the vector potential that determines the function W and, therefore, on the operators \mathcal{L}^\pm . On a different note, the probability density $\rho(x, y, t)$ and probability current $\vec{\mathcal{J}}(x, y, t)$ for an arbitrary state $\Psi(x, y, t)$ associated with the Hamiltonian \mathcal{H} in (2) will be given by

$$\rho(x, y, t) = \Psi^\dagger(x, y, t) \Psi(x, y, t), \quad \vec{\mathcal{J}}(x, y, t) = \Psi^\dagger(x, y, t) \vec{j} \Psi(x, y, t), \quad (19)$$

while the components of probability current \vec{j} turn out to be

$$j_x = \nu v_x \sigma_x, \quad j_y = \nu (v_y \sigma_y + v_t \sigma_0). \quad (20)$$

From now on and unless otherwise indicated, in this work, we will focus on field profiles that lead to eigenfunctions and eigenvalues similar to those obtained in case **i**.

3 Coherent sates

To build the coherent states associated with this system, let us start by assuming the one-dimensional annihilation operator Θ^- acting on the functions ψ_n^- as known, which is such as

$$\begin{aligned}\Theta^- \psi_n^- (x) &= \sqrt{a_n} \psi_{n-1}^- (x), \\ a_0 &= 0, \quad a_n > 0 \quad \text{for } n = 1, 2, \dots\end{aligned}\quad (21)$$

Now, let us introduce a lowering operator for those eigenfunctions in Equation (14) as follows [18]:

$$A^- = \begin{pmatrix} \mathcal{L}^- \frac{1}{\sqrt{H^-}} \Theta^- \frac{f(H^-)}{\sqrt{H^-}} \mathcal{L}^+ & -i \mathcal{L}^- \frac{1}{\sqrt{H^-}} \Theta^- f(H^-) \\ i \Theta^- \frac{f(H^-)}{\sqrt{H^-}} \mathcal{L}^+ & \Theta^- f(H^-) \end{pmatrix}, \quad (22)$$

where f is a real function. Then, the action of A^- on Ψ_n is as follows:

$$A^- \Psi_n(x, y) = 2\sqrt{a_n} f(\epsilon_n^-) \Psi_{n-1}(x, y) \begin{cases} 0 & \text{for } n = 0, \\ \frac{1}{\sqrt{2}} & \text{for } n = 1, \\ 1 & \text{for } n \geq 2. \end{cases} \quad (23)$$

To simplify calculations, we can propose that f is given by:

$$f(\epsilon_n^-) = \frac{\sqrt{g_n}}{2} \times \begin{cases} \sqrt{2} & \text{for } n = 1, \\ 1 & \text{for } n \geq 2. \end{cases} \quad (24)$$

where $g_n := g(n)$, being g a new arbitrary real and positive function. Thus, Equation (17) can be expressed more concisely as:

$$A^- \Psi_n(x, y) = \sqrt{a_n g_n} \Psi_{n-1}(x, y), \quad \forall n. \quad (25)$$

Note that the annihilation operator A^- we have proposed actually represents a family of annihilation operators now labelled by the function g .

3.1 The Barut-Girardello coherent states

There are different definitions that allow us to generalize the concept of coherent states (CS) of the harmonic oscillator. In this work, we consider a coherent state as an eigenstate of the annihilation operator. This type of coherent state is also known as the Barut-Girardello coherent state.

Let $\Psi_\alpha(x, y)$ be the Barut-Girardello coherent state, such that

$$A^- \Psi_\alpha(x, y) = \alpha \Psi_\alpha(x, y), \quad (26)$$

where α is the complex eigenvalue. Since Ψ_α can be represented in the basis of Hamiltonian eigenfunctions

$$\Psi_\alpha(x, y) = \sum_{n=0}^{\infty} d_n \Psi_n(x, y). \quad (27)$$

By substituting (25) into (24) and performing some algebraic manipulations, we get the following recurrence relation

$$\alpha d_{n-1} = \sqrt{a_n g_n} d_n, \quad \text{for } n = 1, 0, \dots \quad (28)$$

which implies that

$$d_n = \frac{\alpha^n d_0}{\sqrt{[a_n]! [g_n]!}}. \quad (29)$$

Here, we have defined the generalized factorial of any arbitrary function f with integer argument n as

$$[f_n]! = \begin{cases} 1 & \text{for } n = 0, \\ f_1 f_2 \cdots f_{n-1} f_n & \text{for } n \geq 1. \end{cases} \quad (30)$$

where $f_n := f(n)$. Thus, the normalized Barut-Girardello coherent state turns out to be:

$$\Psi_\alpha(x, y) = \mathcal{C}_\alpha \sum_{n=0}^{\infty} \frac{\alpha^n}{\sqrt{[a_n]! [g_n]!}} \Psi_n(x, y), \quad (31)$$

being \mathcal{C}_α a normalization constant given by

$$\mathcal{C}_\alpha = \left(\sum_{n=0}^{\infty} \frac{r^{2n}}{[a_n]! [g_n]!} \right)^{-\frac{1}{2}}, \quad (32)$$

where r comes from the polar form for α , i.e., $\alpha = r e^{i\theta}$. It is important to highlight certain key aspects regarding the Barut-Girardello coherent states derived in eq. (29):

- While g_n was initially regarded as an arbitrary function, it is crucial for it to ensure the convergence of the state in equation (29). Consequently, this constrains the family of 'well-behaved' annihilation operators.
- Although the definition of the Barut-Girardello coherent state is not restricted to systems with an infinite-dimensional basis, for those with finite dimensions, the coherent states will coincide with the extremal states (annihilated by A^-), and the corresponding eigenvalue will be zero.

To examine the temporal and phase space behaviors of the Barut-Girardello coherent states (BGCS) of equation (29), we will now use the fidelity and the associated Wigner function.

4 Fidelity and Wigner function

As the concept of coherent states is closely linked to the harmonic oscillator, it is natural to wonder whether BGCS for other physical systems also show well-defined periods of evolution or if their behavior in phase space resembles that of a classical oscillator.

4.1 Fidelity

A method that allows us to determine the possible existence of evolution periods is through fidelity, which is defined as:

$$F(\phi, \xi) \equiv |\langle \phi | \xi \rangle|^2. \quad (33)$$

Thus, if $F(\phi, \xi) = 1$, it can be said that $|\phi\rangle, |\xi\rangle$ differ at most by a global phase factor and both represent the same quantum state. Now, upon applying the time evolution operator $\mathcal{U}(t, 0) = \exp(-i\mathcal{H}t)$ to the coherent state in equation (29), we obtain a state $|\Psi_\alpha(t)\rangle$. After calculating the fidelity with the initial state $|\Psi_\alpha(0)\rangle = |\Psi_\alpha\rangle$, it is determined that

$$F(\Psi_\alpha, \Psi_\alpha(t)) = \mathcal{C}_\alpha^4 \sum_{n,m=0}^{\infty} \frac{r^{2(n+m)}}{[a_n]! [a_m]! [g_n]! [g_m]!} \cos \left[\left(\sqrt{\epsilon_n^-} - \sqrt{\epsilon_m^-} \right) v_x t \right]. \quad (34)$$

The preceding expression indicates that the fidelity between these two states does not depend on the phase of the complex eigenvalue α . On the other hand, due to the argument of the cosine functions that appear in the series, the fidelity never reaches the unity for $t > 0$. This implies that there is no period for which the evolved state returns to its initial state (in contrast to the CS of the harmonic oscillator). Nevertheless, it is always possible to identify certain pseudo-periods for which the states are closer to each other. Additionally, there are some limiting cases ($r < 1$) where the fidelity tends to the unity for some values of t . All these characteristics are illustrated in subsection 4.3.

4.2 Wigner function

To analyze the distribution of the coherent states in phase space, we can utilize the time-dependent Wigner function $W(\mathbf{r}, \mathbf{p}, t)$, which defines a quasiprobability distribution as follows:

$$W(\mathbf{r}, \mathbf{p}, t) = \frac{1}{(2\pi)^n} \int_{-\infty}^{\infty} e^{i\mathbf{p}\cdot\mathbf{r}'} \langle \rho | \mathbf{r} - \frac{\mathbf{r}'}{2} | \mathbf{r} + \frac{\mathbf{r}'}{2} \rangle d\mathbf{r}', \quad (35)$$

where $\rho = |\Psi_\alpha\rangle\langle\Psi_\alpha|$ is the density matrix; $\mathbf{r} = (r_1, r_2, \dots, r_n)$ and $\mathbf{p} = (p_1, p_2, \dots, p_n)$ are n -dimensional vectors representing the classical phase-space position and momentum values. Considering that the wave function for

the CS in equation (29) is defined as $\Psi_\alpha(x, y, t) = \langle \mathbf{r} | \Psi_\alpha(t) \rangle$, then the resulting Wigner function is

$$\begin{aligned} W_\alpha(\mathbf{r}, \mathbf{p}, t) &= W_\alpha(y, p_y) \times W_\alpha(x, p_x, t) \\ &= \delta(p_y - k) \times \frac{C_\alpha^2}{2\pi} \sum_{n,m=0}^{\infty} \frac{r^{n+m} e^{i[(n-m)\theta + (E_n - E_m)t]}}{\sqrt{2^{2-\delta_{n0}-\delta_{m0}} [a_n]! [a_m]! [g_n]! [g_m]!}} \mathcal{M}_{n,m}(x, p_x), \end{aligned} \quad (36)$$

where

$$\mathcal{M}_{n,m}(x, p_x) = \begin{pmatrix} (1 - \delta_{n0})(1 - \delta_{m0}) I_{n-1, m-1}^{+,+}(x, p_x) & -i(1 - \delta_{n0}) I_{n-1, m}^{+, -}(x, p_x) \\ i(1 - \delta_{m0}) I_{n, m-1}^{-, +}(x, p_x) & I_{n, m}^{-, -}(x, p_x) \end{pmatrix}, \quad (37)$$

and

$$I_{n, m}^{\pm, \pm}(x, p_x) = 2 \int_{-\infty}^{\infty} e^{2ip_x z} \psi_n^{\pm}(x - z) \overline{\psi_m^{\pm}(x + z)} dz, \quad (38)$$

here, $\bar{\beta}$ denotes the complex conjugate of a number β and the first (second) superscript \pm along with the subscript n (m) determines the form of the function $\psi_n^{\pm}(x - z)$ ($\psi_m^{\pm}(x + z)$). Let us observe that the coherent state Ψ_α possesses a spinorial nature; this is why a matrix Wigner function is obtained. However, the quasiprobability distribution will be determined by the trace of the matrix from equation (34). In the next subsection, we will present some examples of the phase space behavior of the trace of the Wigner function from equation (34). This will allow us to compare this behavior with that of the CS of the harmonic oscillator.

4.3 Constant magnetic and electric fields

Let us consider a material with an effective Hamiltonian \mathcal{H} as in eq. (2) and localized in the presence of constant magnetic and electric fields given by:

$$\vec{\mathcal{B}} = \mathcal{B}_0 \hat{e}_z, \quad \vec{\mathcal{E}} = -\nu v_t \mathcal{B}_0 \hat{e}_x, \quad (39)$$

where \mathcal{B}_0 is a positive constant, then the scalar and vector potential are given by

$$\vec{\mathcal{A}} = \mathcal{B}_0 x \hat{e}_y, \quad \phi(x) = \nu v_t \mathcal{B}_0 x. \quad (40)$$

This ensures that eq. (9) is satisfied, and the components $\psi_n^{\pm}(x)$ of the eigenstates Ψ_n are identified as eigenfunctions of the supersymmetric Hamiltonians H^{\pm} , which turn out to be

$$H^{\pm} = -\frac{d^2}{dx^2} + \frac{\omega^2}{4} \left(x + \frac{2\tilde{k}}{\omega} \right)^2 \pm \frac{\omega}{2}, \quad (41)$$

where ω and \tilde{k} have been defined as

$$\omega = 2 \frac{v_y}{v_x} \mathcal{B}_0, \quad \tilde{k} = \frac{v_y}{v_x} k. \quad (42)$$

In this way the components ψ_n^{\pm} and the eigenvalue ϵ_n^- turn out to be

$$\psi_n^{\pm}(x) = \sqrt{\frac{1}{2^n n!} \left(\frac{\omega}{2\pi} \right)^{\frac{1}{2}}} H_n \left[\sqrt{\frac{\omega}{2}} \left(x + \frac{2\tilde{k}}{\omega} \right) \right] e^{-\frac{\omega}{4} \left(x + \frac{2\tilde{k}}{\omega} \right)^2}, \quad \epsilon_n^- = n\omega, \quad n = 0, 1, \dots \quad (43)$$

where $H_n(z)$ represents the Hermite polynomial of degree n . As a result, the eigenfunctions of the Hamiltonian \mathcal{H} are given by

$$\Psi_n(x, y) = \frac{e^{iky}}{\sqrt{2^{1-\delta_{n0}}}} \begin{pmatrix} (1 - \delta_{n0}) \psi_{n-1}^-(x) \\ i \psi_n^-(x) \end{pmatrix}, \quad \text{for } n = 0, 1, \dots \quad (44)$$

and the corresponding eigenvalues are $E_n = \nu v_t k + \kappa v_x \sqrt{n\omega}$. Note that since ψ_n^- are the eigenfunctions of the shifted harmonic oscillator and the well-known one-dimensional annihilation operator is given by:

$$\Theta^- = \frac{1}{\sqrt{2}} \left(\zeta + \frac{d}{d\zeta} \right), \quad (45)$$

where $\zeta = \sqrt{\frac{\omega}{2}} \left(x + \frac{2\tilde{k}}{\omega} \right)$, such that

$$\Theta^- \psi_n^-(x) = \sqrt{n} \psi_{n-1}^-(x), \quad \text{for } n = 0, 1, \dots \quad (46)$$

For this case, it is straightforward to see that $a_n = n$ and therefore, the Barut-Girardello coherent states will be given by

$$\Psi_\alpha(x, y) = \mathcal{C}_\alpha \sum_{n=0}^{\infty} \frac{\alpha^n}{\sqrt{n! [g_n]!}} \Psi_n(x, y), \quad (47)$$

with

$$\mathcal{C}_\alpha = \left(\sum_{n=0}^{\infty} \frac{r^{2n}}{n! [g_n]!} \right)^{-\frac{1}{2}}, \quad (48)$$

In this manner, the final form of the BGCS will be dictated by the selection of the function g_n . Next, we will consider two different choices for the function g_n , and in this way, we will determine the behavior of the probability density, probability current, fidelity, and Wigner function for the Barut-Girardello coherent state.

Case $g_n = 1$

If we consider $g_n = 1$, the Barut-Girardello coherent state is reduced to

$$\Psi_\alpha(x, y) = e^{-\frac{r^2}{2}} \sum_{n=0}^{\infty} \frac{r^n e^{in\theta}}{\sqrt{n!}} \Psi_n(x, y), \quad \alpha = r e^{i\theta}. \quad (49)$$

It is straightforward to verify that the states $\Psi_n(x, y)$ follow a Poissonian distribution, $P(n) = |a_n|^2 = e^{-|\alpha|^2} \frac{|\alpha|^{2n}}{n!}$, with the mean equal to $|\alpha|^2$, similar to what happens with coherent states of the harmonic oscillator. Furthermore, we can observe that, algebraically, these states bear a great resemblance to the coherent states of the harmonic oscillator. Nevertheless, their nature differs as, in equation (49), $\Psi_n(x, y)$ represents eigenfunctions of a spinorial type. In Figure 1, we observe the behavior of the probability density, noting how the position of the maximum varies depending on the values of r and θ . In Figure 2, we can observe the behavior of the components of the probability current.

Fidelity

Note that if $g_n = 1$, then the fidelity can be expressed as

$$F(\Psi_\alpha, \Psi_\alpha(t)) = e^{-2r^2} \sum_{n,m=0}^{\infty} \frac{r^{2(n+m)}}{n!m!} \cos [(\sqrt{n} - \sqrt{m}) \sqrt{\omega} v_x t]. \quad (50)$$

As mentioned earlier, the fidelity never reaches the value of unity. However, it is possible to observe certain values of t for which the function reaches local maxima (less than 1). In Figure 3, we can observe how the chosen parameter values determine the time at which these maxima occur. Consequently, there are points on the temporal axis where the fidelity tends to 1 as r approaches zero.

Trace of the time-dependent Wigner matrix function

When $g_n = 1$, the time-dependent Wigner matrix function for the BGCS in eq.(49) turns out to be

$$W_\alpha(\mathbf{r}, \mathbf{p}, t) = \delta(p_y - k) \times \frac{e^{-r^2}}{2\pi} \sum_{n,m=0}^{\infty} \frac{r^{n+m} e^{i[(n-m)\theta + (\sqrt{n} - \sqrt{m})\kappa v_x \sqrt{\omega} t]}}{\sqrt{2^{2-\delta_{n0}-\delta_{m0}} n! m!}} \mathcal{M}_{n,m}(x, p_x), \quad (51)$$

where the functions $I_{n,m}(x, p_x)$ composing the matrix $\mathcal{M}_{n,m}(x, p_x)$ are given by

$$I_{n,m}(x, p_x) = 2e^{-\frac{1}{2}|u|^2} \times \begin{cases} (-1)^m \bar{u}^{n-m} \sqrt{\frac{m!}{n!}} L_n^{n-m}(|u|^2) & \text{for } n \geq m, \\ (-1)^n u^{m-n} \sqrt{\frac{n!}{m!}} L_n^{m-n}(|u|^2) & \text{for } n < m, \end{cases} \quad (52)$$

being L_n^{m-n} the generalized Laguerre polynomials and $u = \sqrt{\omega} \left[\left(x + \frac{2\bar{k}}{\omega} \right) + \frac{2ip}{\omega} \right]$, besides the superscripts \pm in $I_{n,m}$ have been omitted since, for this case, $\psi_n^-(x) = \psi_n^+(x)$. In Figure 4, we can observe the behavior of the trace of the Wigner matrix function at some specific times for a fixed value of the complex eigenvalue α . We can see how the BGCS do not preserve a Gaussian-like distribution in phase space for a long time, as occurs for the coherent states of the harmonic oscillator.

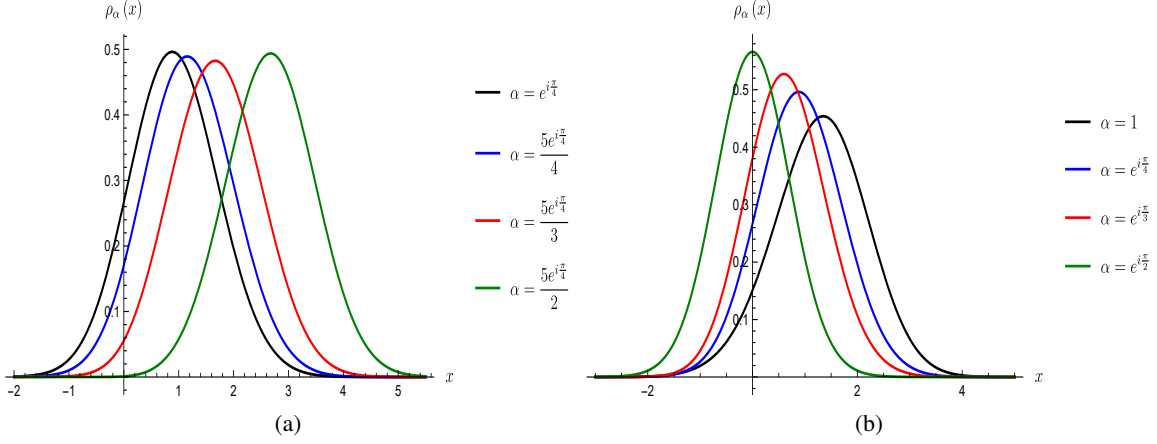


Figure 1: Plots of the probability density for the coherent states given in (49) for $g_n = 1$ as a function of (a) r and (b) θ . The parameters have been taken as $v_x = 0.86$, $v_y = 0.69$, $v_t = 0.32$, $\nu = \kappa = \mathcal{B}_0 = 1$ and $k = 0$.

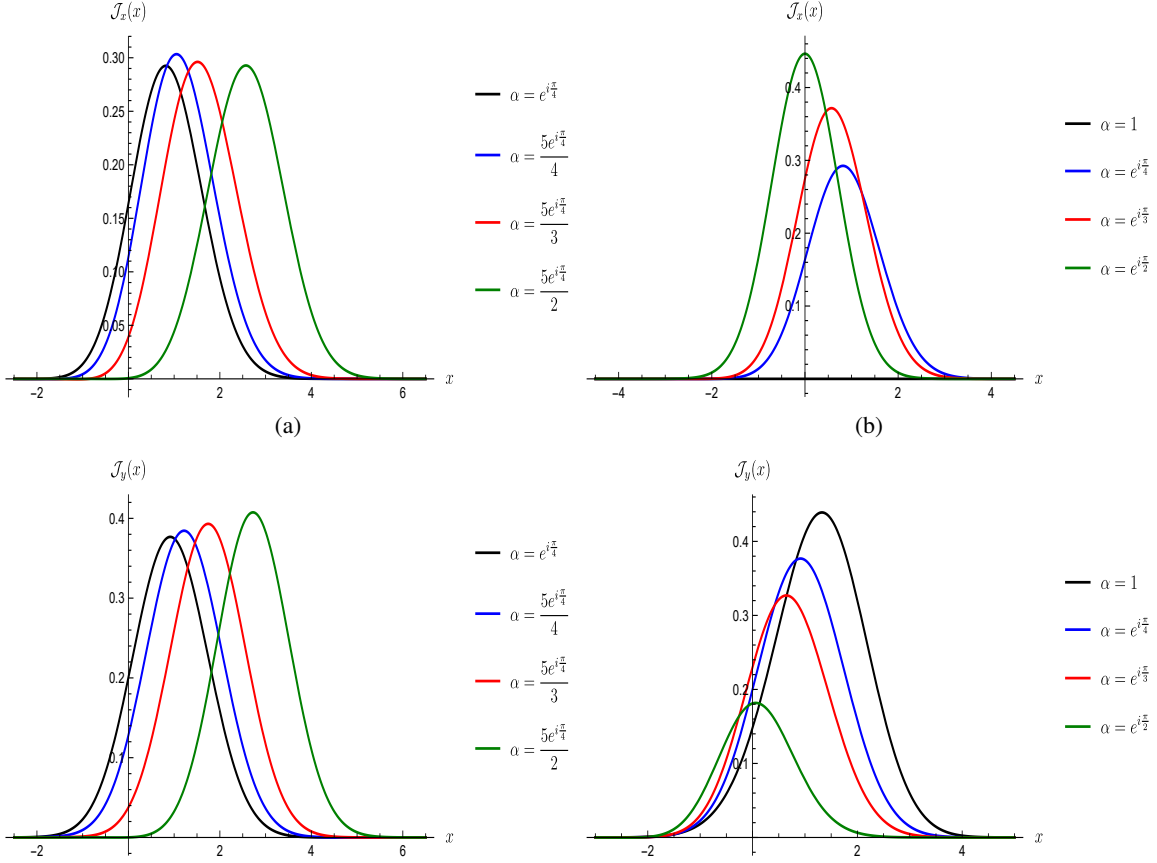


Figure 2: Plots of the x -component of the probability current for the coherent states given in (49) as function of (a) r , (b) θ and the y -component of the probability current as function of (c) r and (d) θ . The parameters have been taken as $v_x = 0.86$, $v_y = 0.69$, $v_t = 0.32$, $\nu = \kappa = \mathcal{B}_0 = 1$ and $k = 0$.

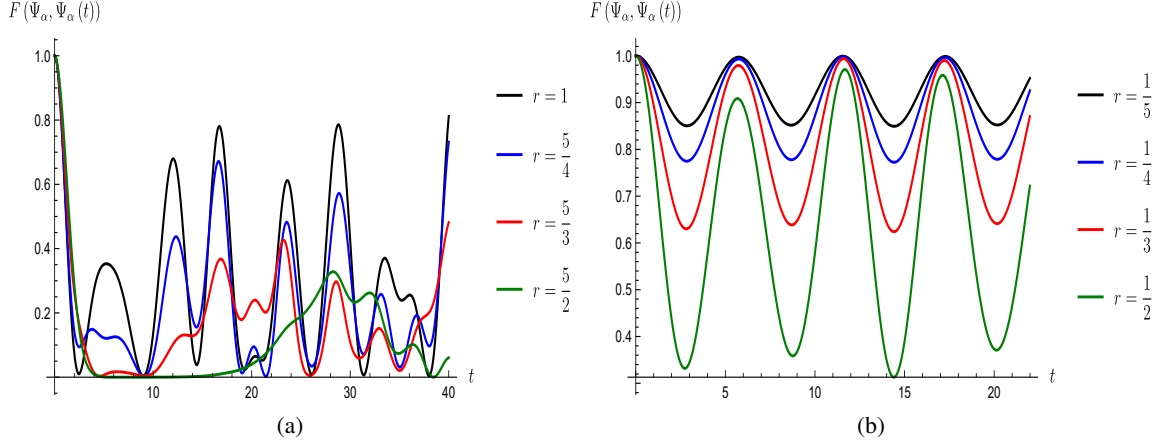


Figure 3: Plots of the fidelity associated with the coherent states of eq. (49) for (a) $r \geq 1$, (b) $r < 1$. The parameters have been taken as $v_x = 0.86$, $v_y = 0.69$, $v_t = 0.32$, $\nu = \kappa = \mathcal{E}_0 = 1$ and $k = 0$.

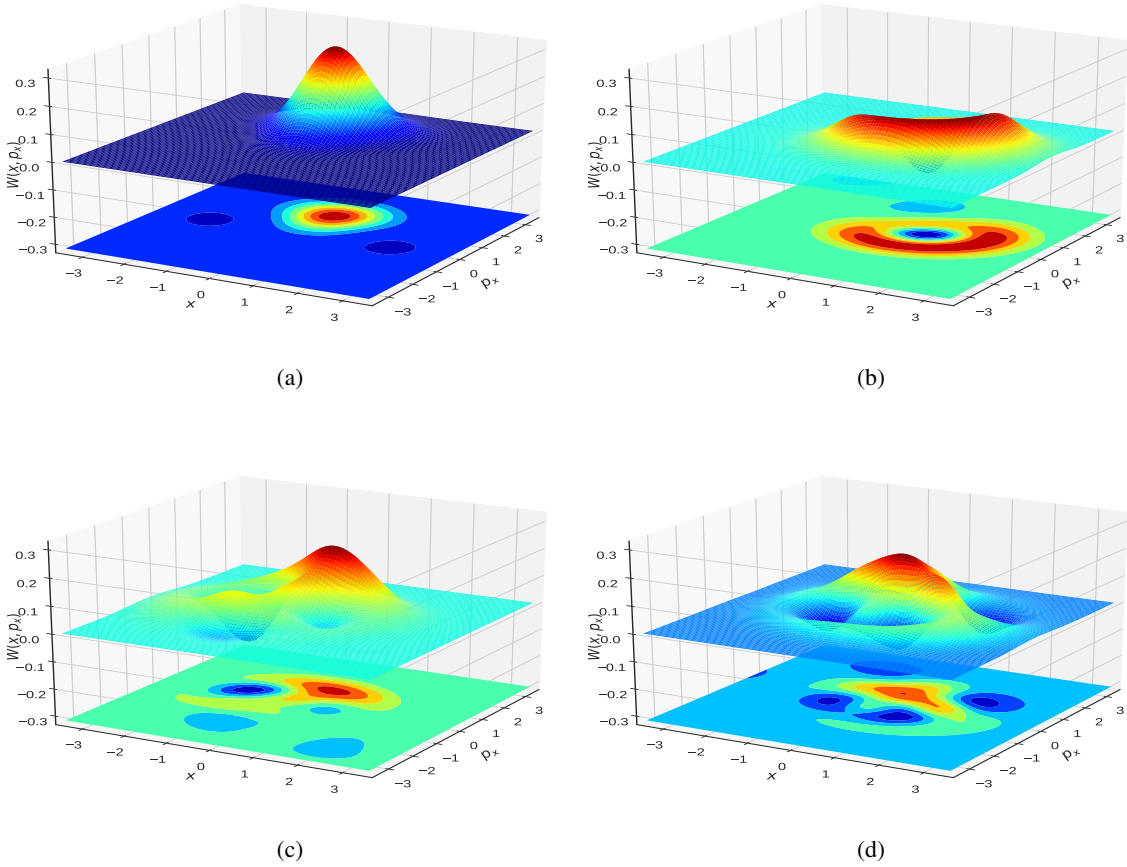


Figure 4: Plots of the trace of the Wigner function given in equation (49). The parameters have been taken as $r = \frac{5}{4}$ and (a) $t = 0$, (b) $t = 3.77$, (c) $t = 16.63$ and (d) $t = 28.86$.

Case $g_n = \frac{1}{n}$

If we consider $g_n = \frac{1}{n}$, the normalization constant C_α for the BGCS in eq. (49) turns out to be

$$C_\alpha = \left(\sum_{n=0}^{\infty} r^{2n} \right)^{-\frac{1}{2}}, \quad (53)$$

which coincides with the square root of the geometric series for r^2 if $r < 1$, thus the BGCS is given by

$$\Psi_\alpha(x, y) = \sqrt{1 - r^2} \sum_{n=0}^{\infty} r^n e^{in\theta} \Psi_n(x, y), \quad \alpha = r e^{i\theta}. \quad (54)$$

It is important to remark this series is only convergent within the unit circle in the complex plane. It is straightforward to verify that the states $\Psi_n(x, y)$ follow a Poissonian distribution, $P(n) = |a_n|^2 = (1 - |\alpha|^2) |\alpha|^{2n}$, which differs from the Poisson distribution obtained for the coherent states of the harmonic oscillator. In Figure 5 and 6, we observe the behavior of the probability density and that of the components of the probability current.

Fidelity

Note that if $g_n = \frac{1}{n}$, then the fidelity can be expressed as

$$F(\Psi_\alpha, \Psi_\alpha(t)) = (1 - r^2)^2 \sum_{n,m=0}^{\infty} r^{2(n+m)} \cos [(\sqrt{n} - \sqrt{m}) \sqrt{\omega} v_x t]. \quad (55)$$

Once again, the fidelity never reaches the unity. Nevertheless, it is possible to identify the local maxima (less than 1) as is shown in Figure 7.

Trace of the time-dependent Wigner matrix function

When $g_n = \frac{1}{n}$, the time-dependent Wigner matrix function for the BGCS in eq.(49) turns out to be

$$W_\alpha(\mathbf{r}, \mathbf{p}, t) = \delta(p_y - k) \times \frac{1 - r^2}{2\pi} \sum_{n,m=0}^{\infty} \frac{r^{n+m} e^{i[(n-m)\theta + (\sqrt{n} - \sqrt{m})\kappa v_x \sqrt{\omega} t]}}{\sqrt{2^{2-\delta_{n0}-\delta_{m0}}}} \mathcal{M}_{n,m}(x, p_x), \quad (56)$$

where the functions $I_{n,m}(x, p_x)$ composing the matrix $\mathcal{M}_{n,m}(x, p_x)$ are given as in eq. (52). In Figure 8, we can observe the behavior of the trace of the Wigner matrix function at some specific times for a fixed value of the complex eigenvalue α . We can see how the BGCS maintain a Gaussian-like shape for a long time, in contrast with those for $g_n = 1$.

5 Conclusions

In this work, we have demonstrated the applicability of supersymmetric quantum mechanics in addressing the eigenvalue problem inherent in Dirac-like materials featuring tilted cones under the influence of electric and magnetic fields, in contrast with previous studies [11–13, 38]. This becomes achievable as long as the presence of the fields permits the elimination of the term connected to the tilting of the cones in the Hamiltonian. A family of lowering operators A^- has been constructed, which is characterized by the function f and built in terms of the intertwining operators typical of SUSY QM. Subsequently, the Barut-Girardello coherent states $\Psi_\alpha(x, y)$ have been represented as eigenvectors of this operator in a basis composed of eigenfunctions of the Hamiltonian. For this set of coherent states, two different families are shown, characterized by the choice of the function g_n . The first of them, with $g_n = 1$, has the characteristic of coinciding with the set obtained by applying the displacement operator $D(\alpha) = e^{\alpha A^+ - \alpha^* A^-}$ ($A^+ = (A^-)^\dagger$) to the ground state $\Psi_0(x, y)$ [18]. On the other hand, the second choice, $g_n = 1/n$, leads us to a family of coherent states that will be convergent if $r < 1$. Then, by calculating the fidelity between the evolved coherent state and its initial state for both cases, we can conclude that the coherent state never returns to its initial state. However, there are certain pseudo-periods, corresponding to local maxima of fidelity, in which these states are approximated more precisely [39]. This behavior is best appreciated when $g_n = 1/n$, given that by having a radius of convergence that requires $|\alpha| < 1$, the coherent state approaches the ground state and the evolution of the latter is well-defined as it is a stationary state. Last but not least, the study of the time-dependent Wigner function allows us

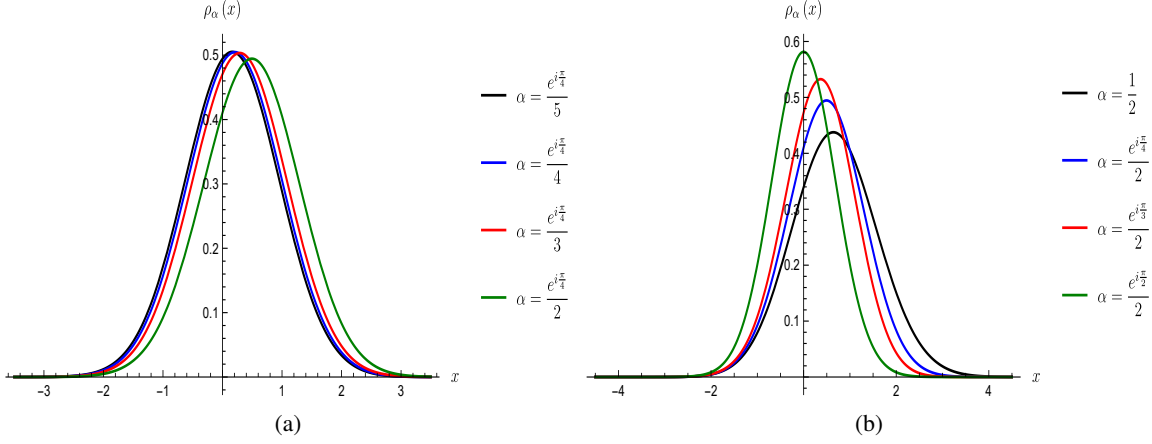


Figure 5: Plots of the probability density for the coherent states given in (54) for $g_n = \frac{1}{n}$ as a function of (a) r and (b) θ . The parameters have been taken as $v_x = 0.86$, $v_y = 0.69$, $v_t = 0.32$, $\nu = \kappa = \mathcal{B}_0 = 1$ and $k = 0$.

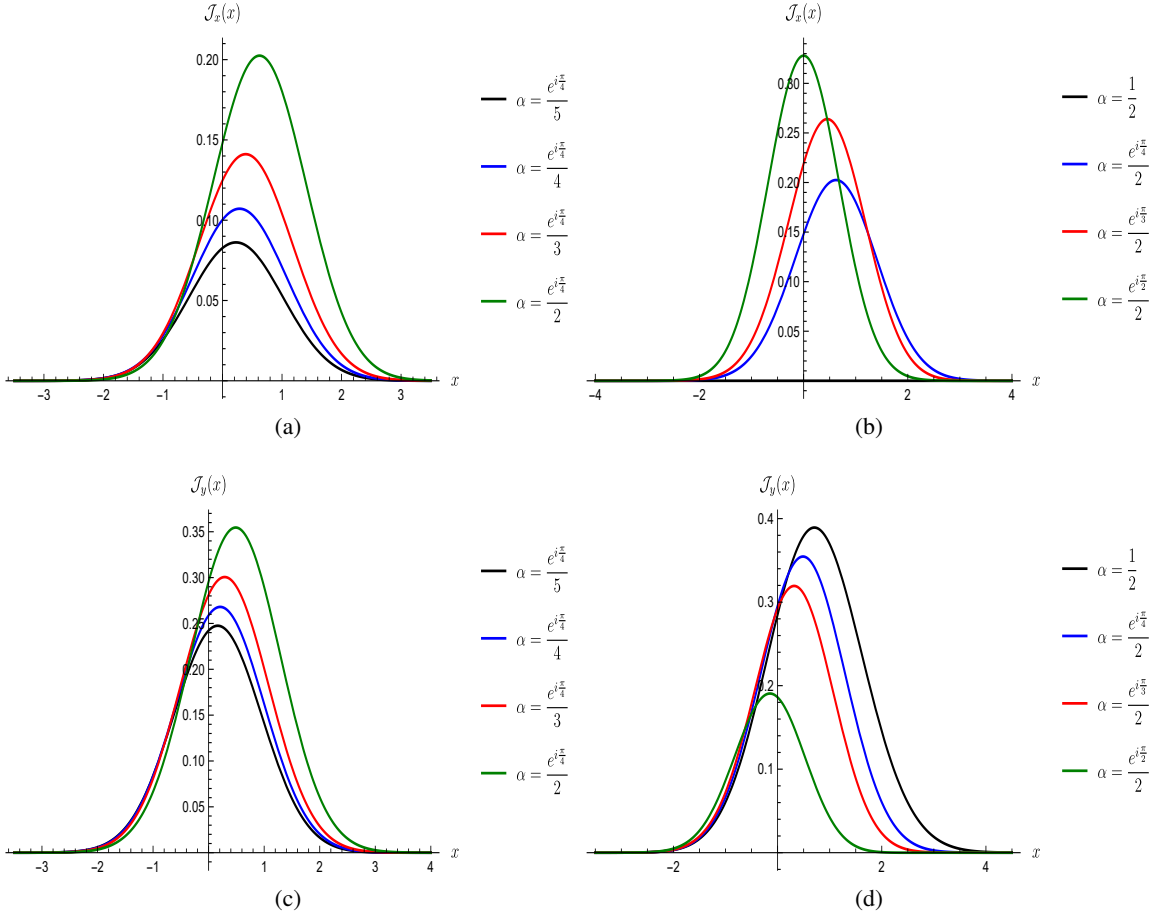


Figure 6: Plots of the x -component of the probability current for the coherent states given in (54) as function of (a) r , (b) θ and the y -component of the probability current as function of (c) r and (d) θ . The parameters have been taken as $v_x = 0.86$, $v_y = 0.69$, $v_t = 0.32$, $\nu = \kappa = \mathcal{B}_0 = 1$ and $k = 0$.

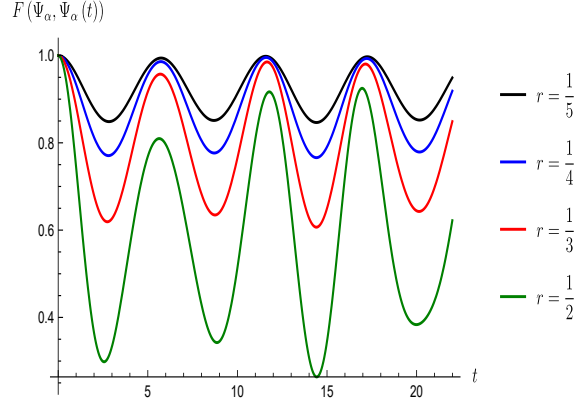


Figure 7: Plot of the fidelity associated with the coherent states of eq. (54) for $r < 1$. The parameters have been taken as $v_x = 0.86$, $v_y = 0.69$, $v_t = 0.32$, $\nu = \kappa = \mathcal{B}_0 = 1$ and $k = 0$.

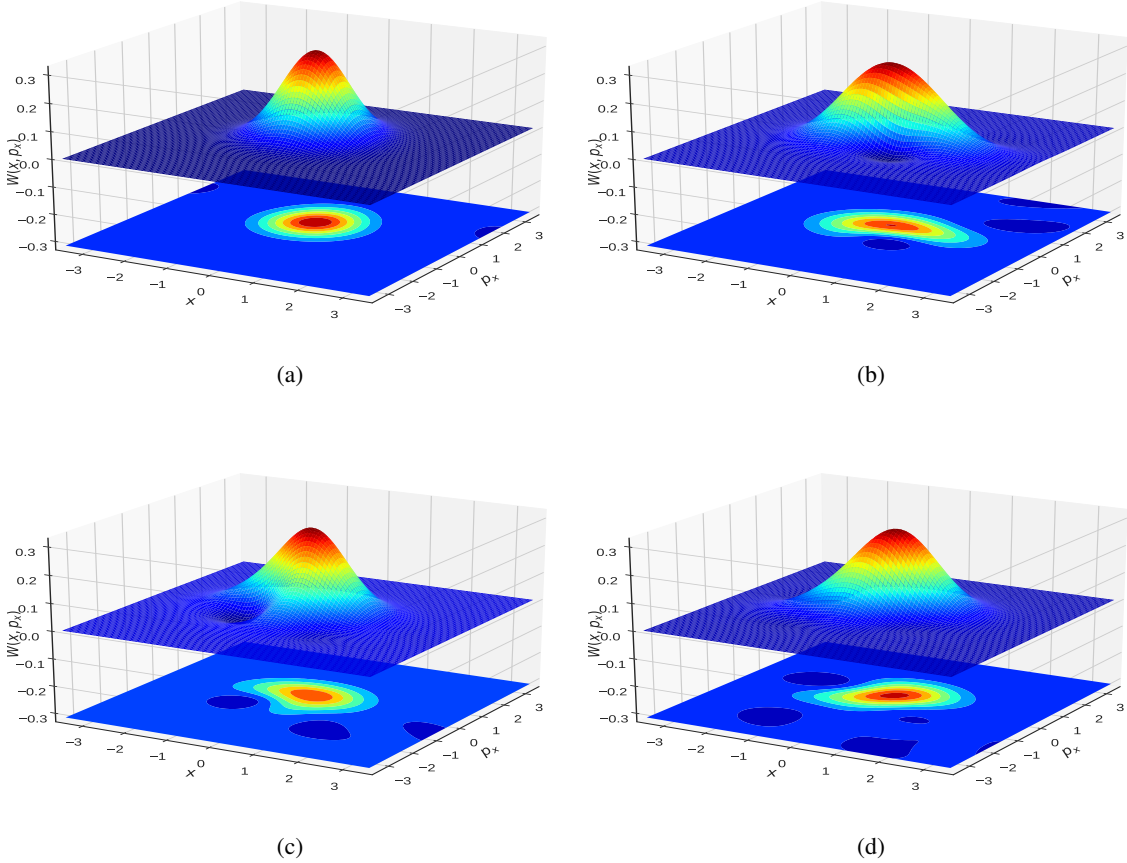


Figure 8: Plots of the trace of the Wigner function given in equation (54). The parameters have been taken as $r = \frac{1}{2}$ and (a) $t = 0$, (b) $t = 5.63$, (c) $t = 11.77$ and (d) $t = 16.95$.

to contrast the distribution of coherent states in phase space with what would be expected (a Gaussian distribution) for a standard coherent state of the harmonic oscillator. As can be seen in Figure 4, coherent states with $g_n = 1$ only maintain a Gaussian-like shape for their initial state, but as it evolves, the distribution takes negative values, which is

an indication that such states increase their quantumness. In contrast, the family of coherent states with $g_n = 1/n$ is more stable in time, i.e., it preserves its classicality for a large time (see Figure 8). From the time evolution of the Wigner function, we can infer the coherent states in equation (49) do not saturate the Heisenberg uncertainty relation for $t > 0$, while those in (54) seem to minimize the position and momentum uncertainty for a large time, becoming the most classical states here shown. Finally, it is worth mentioning that the choice made about g_n will affect the way the coherent state evolves over time.

Acknowledgments. The authors acknowledge financial support from CONAHCYT Project FORDECYT-PRONACES/61533/2020. DOC acknowledges the support of CONAHCYT through the postdoctoral fellowship with the CVU number 712322. EDB also acknowledges the SIP-IPN research grant 20242347.

References

- [1] Y. Zhao, X. Li, J. Liu, C. Zhang, and Q. Wang, “A New Anisotropic Dirac Cone Material: A B2S Honeycomb Monolayer,” *J. Phys. Chem. Lett.*, vol. 9, no. 7, pp. 1815–1820, 2018.
- [2] B. Feng, J. Zhang, R.-Y. Liu, T. Iimori, C. Lian, H. Li, L. Chen, K. Wu, S. Meng, F. Komori, and I. Matsuda, “Direct evidence of metallic bands in a monolayer boron sheet,” *Phys. Rev. B*, vol. 94, p. 041408, Jul 2016.
- [3] A. J. Mannix, X.-F. Zhou, B. Kiraly, J. D. Wood, D. Alducin, B. D. Myers, X. Liu, B. L. Fisher, U. Santiago, J. R. Guest, M. J. Yacaman, A. Ponce, A. R. Oganov, M. C. Hersam, and N. P. Guisinger, “Synthesis of borophenes: Anisotropic, two-dimensional boron polymorphs,” *Science*, vol. 350, p. 1513, dec 2015.
- [4] A. Lopez-Bezanilla and P. B. Littlewood, “Electronic properties of 8–*Pmmn* borophene,” *Phys. Rev. B*, vol. 93, p. 241405, jun 2016.
- [5] M. O. Goerbig, J.-N. Fuchs, G. Montambaux, and F. Piéchon, “Electric-field-induced lifting of the valley degeneracy in α -(BEDT-TTF)₂I₃ Dirac-like Landau levels,” *EPL*, vol. 85, p. 57005, mar 2009.
- [6] M. I. Katsnelson, *Graphene: Carbon in Two Dimensions*. Cambridge: Cambridge University Press, 2012.
- [7] T. Cheng, H. Lang, Z. Li, Z. Liu, and Z. Liu, “Anisotropic carrier mobility in two-dimensional materials with tilted Dirac cones: theory and application,” *Phys. Chem. Chem. Phys.*, vol. 19, pp. 23942–23950, 2017.
- [8] J. R. Schaibley, H. Yu, G. Clark, P. Rivera, J. S. Ross, K. L. Seyler, W. Yao, and X. Xu, “Valleytronics in 2D materials,” *Nature Reviews Materials*, vol. 1, no. 11, p. 16055, 2016.
- [9] Y. S. Ang, S. A. Yang, C. Zhang, Z. Ma, and L. K. Ang, “Valleytronics in merging Dirac cones: All-electric-controlled valley filter, valve, and universal reversible logic gate,” *Phys. Rev. B*, vol. 96, p. 245410, Dec 2017.
- [10] M. S. Mrudul, Álvaro Jiménez-Galán, M. Ivanov, and G. Dixit, “Light-induced valleytronics in pristine graphene,” *Optica*, vol. 8, pp. 422–427, Mar 2021.
- [11] E. Díaz-Bautista and Y. Betancur-Ocampo, “Phase-space representation of Landau and electron coherent states for uniaxially strained graphene,” *Phys. Rev. B*, vol. 101, p. 125402, mar 2020.
- [12] E. Díaz-Bautista, “About the time evolution of coherent electron states in monolayers of boron allotropes,” *Acta Polytech.*, vol. 62, no. 1, pp. 38–49, 2022.
- [13] Y. Betancur-Ocampo, E. Díaz-Bautista, and T. Stegmann, “Valley-dependent time evolution of coherent electron states in tilted anisotropic Dirac materials,” *Phys. Rev. B*, vol. 105, p. 045401, Jan 2022.
- [14] Ş. Kuru, J. Negro, and L. M. Nieto, “Exact analytic solutions for a Dirac electron moving in graphene under magnetic fields,” *J. Phys. Condens. Matter*, vol. 21, p. 455305, oct 2009.
- [15] B. Midya and D. J. Fernández, “Dirac electron in graphene under supersymmetry generated magnetic fields,” *J. Phys. A Math. Theor.*, vol. 47, p. 285302, jun 2014.
- [16] D. J. Fernández, J. D. García-Muñoz, and D. O-Campa, “Electron in bilayer graphene with magnetic fields leading to shape invariant potentials,” *J. Phys. A Math. Theor.*, vol. 53, p. 435202, oct 2020.
- [17] D. J. Fernández, J. D. García-Muñoz, and D. O-Campa, “Bilayer graphene in magnetic fields generated by supersymmetry,” *J. Phys. A Math. Theor.*, vol. 54, p. 245302, may 2021.
- [18] D. J. Fernández C. and D. O-Campa, “Graphene generalized coherent states,” *Eur. Phys. J. Plus*, vol. 137, p. 1012, Sep 2022.
- [19] E. Wigner, “On the quantum correction for thermodynamic equilibrium,” *Phys. Rev.*, vol. 40, p. 749, jun 1932.
- [20] W. B. Case, “Wigner functions and Weyl transforms for pedestrians,” *Am. J. Phys.*, vol. 76, p. 937, oct 2008.

- [21] M. V. Berry, “Semi-classical mechanics in phase space: A study of Wigner’s function,” *Philosophical Transactions of the Royal Society of London. Series A, Mathematical and Physical Sciences*, vol. 287, p. 237, oct 1977.
- [22] A. Kenfack and K. Zyczkowski, “Negativity of the Wigner function as an indicator of non-classicality,” *J. Opt. B: Quantum Semiclassical Opt.*, vol. 6, p. 396, aug 2004.
- [23] D. T. Smithey, M. Beck, M. G. Raymer, and A. Faridani, “Measurement of the Wigner distribution and the density matrix of a light mode using optical homodyne tomography: Application to squeezed states and the vacuum,” *Phys. Rev. Lett.*, vol. 70, p. 1244, mar 1993.
- [24] M. Hillery, R. O’Connell, M. Scully, and E. Wigner, “Distribution functions in physics: Fundamentals,” *Phys. Rep.*, vol. 106, p. 121, apr 1984.
- [25] C. K. Zachos, D. B. Fairlie, and T. L. Curtright, *Quantum Mechanics in Phase Space*. World Scientific, 2005.
- [26] F. Bayen, M. Flato, C. Fronsdal, A. Lichnerowicz, and D. Sternheimer, “Deformation theory and quantization. I. Deformations of symplectic structures,” *Annals of Physics*, vol. 111, no. 1, pp. 61–110, 1978.
- [27] F. Bayen, M. Flato, C. Fronsdal, A. Lichnerowicz, and D. Sternheimer, “Deformation theory and quantization. II. Physical applications,” *Annals of Physics*, vol. 111, no. 1, pp. 111–151, 1978.
- [28] M. Bordemann, “Deformation quantization: a survey,” *Journal of Physics: Conference Series*, vol. 103, p. 012002, feb 2008.
- [29] J. Weinbub and D. K. Ferry, “Recent advances in Wigner function approaches,” *Appl. Phys. Rev.*, vol. 5, p. 041104, dec 2018.
- [30] J. Weinbub and R. Kosik, “Computational perspective on recent advances in quantum electronics: from electron quantum optics to nanoelectronic devices and systems,” *Journal of Physics: Condensed Matter*, vol. 34, p. 163001, feb 2022.
- [31] D. Leibfried, T. Pfau, and C. Monroe, “Shadows and Mirrors: Reconstructing Quantum States of Atom Motion,” *Physics Today*, vol. 51, pp. 22–28, 04 1998.
- [32] A. Bertoni, P. Bordone, R. Brunetti, and C. Jacoboni, “The Wigner function for electron transport in mesoscopic systems,” *Journal of Physics: Condensed Matter*, vol. 11, p. 5999, aug 1999.
- [33] C. Jacoboni and P. Bordone, “The Wigner-function approach to non-equilibrium electron transport,” *Reports on Progress in Physics*, vol. 67, p. 1033, jun 2004.
- [34] T. Jullien, P. Roulleau, B. Roche, A. Cavanna, Y. Jin, and D. C. Glatli, “Quantum tomography of an electron,” *Nature*, vol. 514, p. 603, oct 2014.
- [35] R. Bisognin, A. Marguerite, B. Roussel, M. Kumar, C. Cabart, C. Chapdelaine, A. Mohammad-Djafari, J.-M. Berroir, E. Bocquillon, B. Plaçais, A. Cavanna, U. Gennser, Y. Jin, P. Degiovanni, and G. Fève, “Quantum tomography of electrical currents,” *Nature Communications*, vol. 10, p. 3379, 2019.
- [36] J. D. Fletcher, N. Johnson, E. Locane, P. See, J. P. Griffiths, I. Farrer, D. A. Ritchie, P. W. Brouwer, V. Kashcheyevs, and M. Kataoka, “Continuous-variable tomography of solitary electrons,” *Nature Communications*, vol. 10, p. 5298, 2019.
- [37] B. Roussel, C. Cabart, G. Fève, and P. Degiovanni, “Processing quantum signals carried by electrical currents,” *PRX Quantum*, vol. 2, p. 020314, May 2021.
- [38] J. A. Mojica-Zárata, D. O-Campa, and E. Díaz-Bautista, “An algorithm for exact analytical solutions for tilted anisotropic dirac materials,” *Eur. Phys. J. Plus*, vol. 139, p. 272, Mar 2024.
- [39] D. J. Fernández and D. I. Martínez-Moreno, “Bilayer graphene coherent states,” *Eur. Phys. J. Plus*, vol. 135, p. 739, sep 2020.